

# Growth of III–N materials and devices by metalorganic chemical vapor deposition

© R.D. Dupuis<sup>†</sup> ¶, P.A. Grudowski<sup>†</sup>, C.J. Eiting<sup>†,\*</sup>, J. Park<sup>†</sup>

<sup>†</sup> The University of Texas at Austin, Microelectronics Research Center  
PRC/MER 1.606D–R9900 Austin TX 78712-1100 USA

\* The Air Force Research Laboratory, Materials and Manufacturing Directorate,  
WPAFB OH 45433-7707 USA

(Получена 1 марта 1999 г. Принята к печати 2 марта 1999 г.)

The characteristics of III–V nitride semiconductor epitaxial layers grown by metalorganic chemical vapor deposition are of interest for the realization of many technologically important devices. This paper will review heteroepitaxial growth on (0001) sapphire substrates as well as the selective-area and subsequent lateral epitaxial overgrowth on masked substrate surfaces.

## 1. Introduction to semiconducting nitrides

The growth of high-quality III–V nitride semiconductor epitaxial films is a recent development dating from about 1989 with the work of Akasaki, et al. [1]. Because of its large direct bandgap extending from ultraviolet (UV) (6 eV) through the entire visible spectrum to red (2 eV), the indium aluminum gallium nitride (InAlGaN) system has great potential for many different optoelectronic and electronic devices. Already, extensive work has been carried out on visible light emitting diodes (LED's) [2,3], injection laser diodes (LD's) [4–9], UV photodetectors [10,11], and field-effect transistors [12].

Compound semiconductors in the nitride material system can be grown in both the cubic (zinc blende) and hexagonal (wurtzite) crystalline forms, although the wurtzite form is the preferred metastable state of InAlGaN alloys. The source of many of the problems associated with the growth of high-quality nitride films is the lack of a lattice-matched substrate. While commercially viable substrates such as cubic Si and GaAs have been used with limited success, the substrates of choice have been hexagonal c-plane (0001) sapphire (Al<sub>2</sub>O<sub>3</sub>) and the hexagonal form of silicon carbide (6H-SiC). Recently, alternative approaches to heteroepitaxial growth using selective-area growth have been developed for high-quality nitride films. We will review recent progress in this field.

## 2. MOCVD growth of III–N films

The largest advance in the research on nitride semiconductors was the development of the buffer layer growth prior to deposition of the single crystal GaN. Yoshida et al., using molecular-beam epitaxy (MBE), first discovered this "two-step" growth process [13]. Akasaki, et al., employed this idea using metalorganic chemical vapor deposition (MOCVD) and extensively studied the effect of a thin (50 ÷ 100 nm)

low-temperature (600°C) intermediate AlN layer when growing GaN on sapphire [1]. This group showed from X-ray diffraction studies that the mosaicity and therefore the defect structure related to the degree of mosaicity, of the GaN epitaxial layers was reduced by using the AlN buffer layer and proposed a model in which the initial deposition results in small AlN crystallites that combine to form an amorphous layer. As GaN is deposited on this amorphous buffer layer, three-dimensional islands begin to form, but eventually coalesce to form a smooth, continuous layer. The coalescence is enhanced by a reduction of the interfacial free energy between GaN and AlN. The highly defective buffer layer tended to "absorb" a lot of the strain and reduced the number of dislocations extending to the surface of the epitaxial layer grown on top of it. Deposition without the buffer layer results in large three dimensional islands which eventually join and form heavily boundary regions throughout the layer.

Nakamura adapted this process to a two-step growth technique that does not require the use of AlN. Using atmospheric-pressure MOCVD, he was able to obtain the same beneficial effects of an AlN buffer layer by using GaN low-temperature layer. In fact, with 20 nm GaN buffer layer, he achieved higher electron mobilities, lower background electron concentrations, and lower X-ray FWHM values than for GaN grown on an AlN buffer layer [1].

All of the materials discussed in this work were grown at the University of Texas at Austin by metalorganic chemical vapor deposition in the EMCORE D125 vertical geometry, rotating disk MOCVD reactor. The system is capable of using 6 hydride sources for group V and dopant precursors and 10 metalorganic sources for group III and dopant precursors. The hydrides are ammonia for the group V nitrogen source and the mixture of 50 ppm silane (SiH<sub>4</sub>) in hydrogen (H<sub>2</sub>) for the silicon dopant source. The group III metalorganics used are trimethylgallium (TMGa), triethylgallium (TEGa), trimethylaluminum (TMAI), and trimethylindium (TMIn). The dopant source is bis(cyclopentadienyl)magnesium (Cp<sub>2</sub>Mg).

¶ E-mail: dupuis@mail.utexas.edu

## 2.1. Si-doped and Mg-doped GaN

To date, the best doping success in GaN has been achieved with silicon (*n*-type) and magnesium (*p*-type) dopant atoms. We have achieved *n*-type silicon doping with electron carrier concentrations ranging from  $n = 5 \cdot 10^{17}$  to  $1 \cdot 10^{19} \text{ cm}^{-3}$  and maximum electron mobility  $\sim 300 \text{ cm}^2/\text{V}\cdot\text{s}$  for  $n = 2 \cdot 10^{18} \text{ cm}^{-3}$ . Fig. 1 shows the relationship between the electron carrier concentration and resistivity, as determined by room-temperature Hall effect measurements, and the  $\text{SiH}_4$  molar flow. The carrier concentration is very linear with dopant molar flow, indicative of constant dopant atom activation even at higher flows. The resistivity, however, obeys the non-linear relationship at higher flows due to decrease in the electron mobility. The mobility decrease with higher carrier concentration is an expected effect due to the higher degree of impurity scattering.

*P*-type doping with magnesium has also been demonstrated, however, the 300 K free-hole carrier concentrations for GaN:Mg films range from  $p \simeq 7 \cdot 10^{15}$  to  $2 \cdot 10^{18} \text{ cm}^{-3}$  with maximum hole mobility of  $13 \text{ cm}^2/\text{V}\cdot\text{s}$ . These

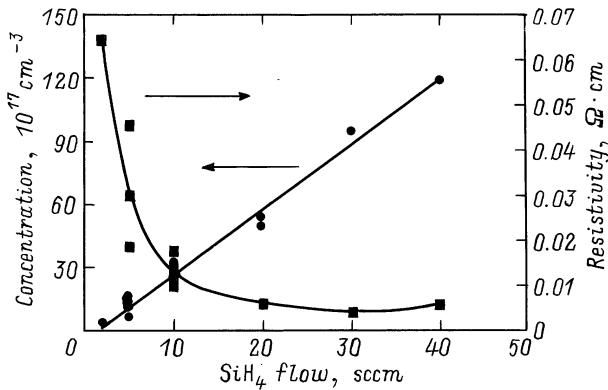


**Figure 1.** Room-temperature Hall-effect data for Si-doped GaN films showing the relationship between electron carrier concentration and film resistivity versus the input  $\text{SiH}_4$  mixture bulk flow.

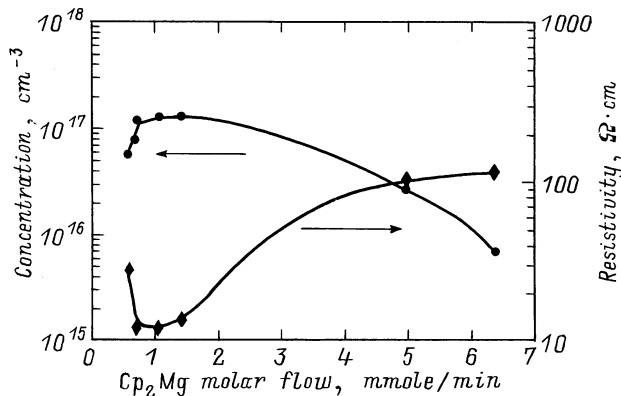


**Figure 2.** Room-temperature Hall effect data for Mg-doped GaN films showing the relationship between electron carrier concentration and film resistivity versus the input  $\text{Cp}_2\text{Mg}$  molar flow.

samples were obtained by optimizing the  $\text{Cp}_2\text{Mg}$  molar flow and thermally activating Mg atoms with a post growth *in-situ* (growth chamber) or *ex-situ* (rapid thermal annealing furnace)  $\text{N}_2$  ambient activation anneal at  $700 \div 1000^\circ\text{C}$  for  $10 \div 30$  min. Fig. 2 shows the 300 K Hall effect results for the hole carrier concentration and resistivity versus  $\text{Cp}_2\text{Mg}$  molar flow.

## 2.2. Growth of multiple quantum well heterostructures

After achieving the growth of *n*-type and *p*-type materials, we studied the growth of the AlGaN and InGaN epitaxial layers and heterojunctions required for high-efficiency LED's and injection lasers. These structures were designed to become the light-confining and light-emitting component of the device structure. An important issue we investigated was the structure of the multiple quantum well (MQW) active region. Multiple quantum wells are chosen over a single quantum well to increase the luminescence intensity of the structures. Obviously, increase of the number of emitting layers will increase the total number of electron-hole pairs and, therefore, the number of emitted photons. The tradeoff in the nitride material system involves the excess strain induced by heteroepitaxial growth. The higher In content in InGaN and the thicker the overall active region, the more strain exists. Finally, if the critical layer thickness is approached, relaxation of the layers occurs and defect generation is enhanced. All of the MQW regions reported here have the total thickness, which should be much below the critical layer thickness of InGaN alloys. The effect of varying the number of periods in the MQW structure consisting of  $35 \text{ \AA}$   $\text{In}_{0.13}\text{Ga}_{0.87}\text{N}$  quantum wells and  $70 \text{ \AA}$   $\text{In}_{0.03}\text{Ga}_{0.97}\text{N}$  barrier was investigated. We determined that the optimum structure was a 5-period MQW for this well/barrier combination.

With this MQW optimized in terms of the Si doping level and the number of periods, AlGaN cladding layers were added to the photoluminescence (PL) structure to examine the effect of increased overall strain in the samples. Laser-diode structures require some type of AlGaN cladding layers for effective carrier and optical confinement, because of the band offsets and refractive index steps between GaN, InGaN, and AlGaN. However, adding AlGaN thick layers with low Al content will increase the amount of heteroepitaxial strain on the structure. The 300 K PL data in Fig. 3 show the effect of adding a 150 nm Si-doped  $\text{Al}_{0.10}\text{Ga}_{0.90}\text{N}$  lower cladding (below the MQW active region) and a 20 nm  $\text{Al}_{0.10}\text{Ga}_{0.90}\text{N}$  cap to the optimized MQW PL structure. The upper cladding, or cap, had to be thin in PL structures. This data shows that there is absolutely no strain-induced degradation caused by the added AlGaN. The MQW luminescence peak intensity, and FWHM are nearly identical for both samples.

X-ray diffraction is used primarily on these samples to verify the period thickness of the MQW region and to confirm InGaN and AlGaN alloy compositions. By measuring the spacing of the superlattice satellite peaks,

an accurate measurement of the period thickness can be made. Shown in Fig. 4 is the (00•6) reflection  $\omega - 2\theta$  curve for two different MQW active regions. From this data and the formula for X-ray diffraction from a period structure, the period thickness measured from the spacing between the 0th order and -1st order satellite peaks for sample *a* was 101 Å and for sample *b* was 106 Å. The intended period thickness was 105 Å for both samples, so the agreement is quite good and very reproducible from sample to sample. This shows that growth rates obtained from the growth and scanning electron microscopy characterization of thick ( $\sim 100$  nm) InGaN layers are very accurate down to the short growth times required for well and barrier thicknesses. Also notice that the 0th order peak for curve *b* is slightly further separated from the GaN peak than for

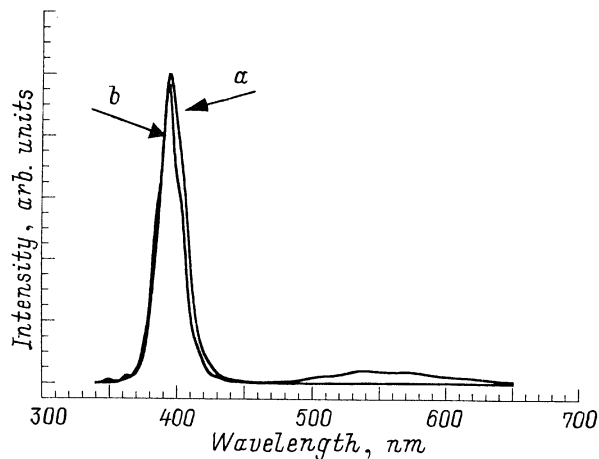


**Figure 3.** Room-temperature PL spectra for MQW structures grown at 830°C, consisting of 35 Å  $\text{In}_{0.13}\text{Ga}_{0.87}\text{N}$  quantum wells and 70 Å  $\text{In}_{0.03}\text{Ga}_{0.97}\text{N}$  barriers, doped with 20 sccm  $\text{SiH}_4$ , and (a) without or (b) with upper and lower  $\text{Al}_{0.10}\text{Ga}_{0.90}\text{N}:\text{Si}$  cladding layers. FWHM: *a* — 174 meV, *b* — 170 meV.

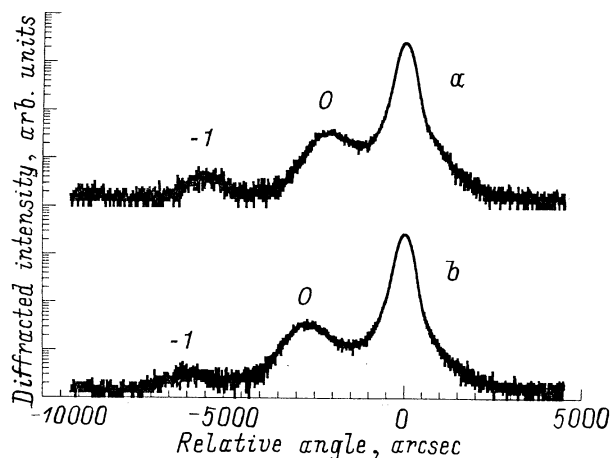


**Figure 4.** X-ray  $\omega - 2\theta$  (00•6) curves for MQW active regions consisting of (a) 35 Å  $\text{In}_{0.13}\text{Ga}_{0.87}\text{N}$  quantum wells, 70 Å  $\text{In}_{0.03}\text{Ga}_{0.97}\text{N}$  barriers and (b) 42 Å  $\text{In}_{0.15}\text{Ga}_{0.85}\text{N}$  quantum wells, 63 Å  $\text{In}_{0.05}\text{Ga}_{0.95}\text{N}$  barriers.

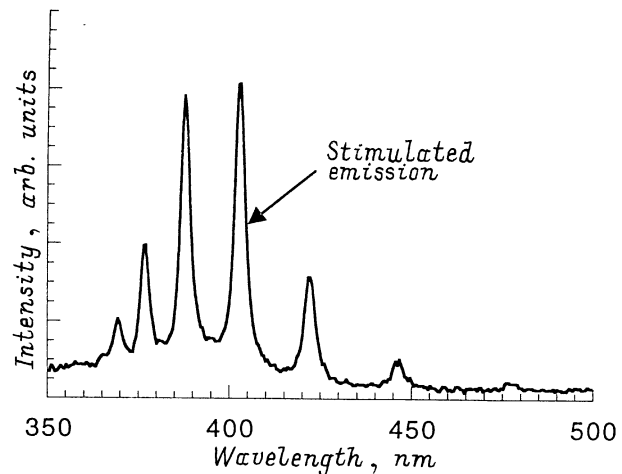


**Figure 5.** Stimulated emission spectrum for photopumped (pulsed  $\text{N}_2$  laser) MQW structure consisting of five periods of 42 Å  $\text{In}_{0.15}\text{Ga}_{0.85}\text{N}$  quantum well and 63 Å  $\text{In}_{0.05}\text{Ga}_{0.95}\text{N}$  barrier.

curve *a*. This peak corresponds to the average indium content of the MQW. The average indium content of *b* is larger because the indium content of the well and barrier is slightly higher (15 and 5% compared to 13 and 3%) and the fraction of the well thickness to the overall thickness is higher (43/105 compared to 30/105). So, again, the X-ray diffraction data are in good agreement with the structure that we intended to grow.

The material quality of the MQW active region has been qualified by performing 300 K high-intensity photopumping experiments. Photopumping provides the high power densities needed for population inversion in the active region without the need for electrical injection through doped layers. Therefore, a qualitative analysis of the active region's potential for achieving stimulated emission is possible without having to worry about internal heating in the structure due to resistive current paths or about defect induced degradation due to complicated epitaxial layer structures. Fig. 5 shows the results of the photopumping experiment on the MQW PL structure corresponding an optimized MQW active region. This experiment was performed with a pulsed (frequency  $f < 100$  Hz) nitrogen laser capable of providing several  $\text{MW}/\text{cm}^2$  peak power density. Attenuators were placed in the beam to reduce the optical energy incident upon the sample. The luminescence recorded emitting from the surface of the sample (perpendicular to the growth plane) clearly shows significant narrowing to the linewidth at the characteristic wavelength of  $\lambda = 400$  nm, which is a good indication of stimulated emission. Also, Fabry–Perot cavity modes, whose spacing corresponds roughly to the vertical thickness of the entire epitaxial structure ( $\sim 1.5 \mu\text{m}$ ) are evident. The air/semiconductor interface and the semiconductor/substrate interface create the vertical cavity. We also conclude from the change in slope of the sample output power versus, relative pump input power data that this material is operating under stimulated emission conditions.

### 2.3. Selective-area and lateral epitaxial overgrowth

Joyce and Baldrey first demonstrated selective-area epitaxy (SAE) of semiconductors in 1962. They demonstrated SAE of Si using  $\text{SiO}_2$  masks and  $\text{SiCl}_4$  as a precursor [14]. An extension of this work, SAE and subsequent lateral epitaxial overgrowth (LEO) of a semiconductor film over the mask has also been reported for a variety of materials [15]. Recently, Davis et al. [16–18] have reported using MOCVD for the selective-area lateral epitaxial overgrowth (SALEO) of GaN on 6H-SiC substrates and have reported that the portion of the GaN film grown over the oxide mask has a reduced density of threading dislocations. More recently, Nakamura et al. have reported employing the SALEO process to grow complete AlGaIn/InGaIn/GaN injection laser device structures having a greatly improved reliability performance due to the reduction of the density of threading dislocations in the active region which is located in the SAE portion of the layer grown directly over the mask openings [19]. The dislocation structure of these LEO materials is of great interest and it is reported to be lower by over two orders of magnitude than the materials grown directly on sapphire substrates [20]. While these demonstrations of high-quality III–N materials have resulted in an increased interest in the SALEO process, not many reports of the dependence of the details of the GaN SALEO upon growth conditions have been published.

The SALEO films in this study are grown at the pressure  $\sim 100$  Torr and at the temperatures in the range  $1030 \leq T_g \leq 1100^\circ\text{C}$ . The GaN heteroepitaxial "substrates" are prepared by growing  $\sim 2\ \mu\text{m}$  of GaN on (0001) sapphire by MOCVD at  $T_g \simeq 1050^\circ\text{C}$ . Next, an  $\sim 100$  nm thick  $\text{SiO}_2$  mask is deposited by plasma-enhanced chemical vapor deposition (PECVD) using  $\text{SiH}_4$  and  $\text{N}_2\text{O}$  precursors. Conventional optical lithography and wet chemical etching are used to produce various stripe patterns in the  $\text{SiO}_2$  mask layer.

We have achieved smooth vertical sidewalls and rectangular cross section GaN SALEO mesas for mask stripes oriented along the  $\langle 1\bar{1}00 \rangle$  direction while triangular cross section mesas are obtained for stripes parallel to the  $\langle 11\bar{2}0 \rangle$  direction. The mesas with a rectangular cross section have surfaces bounded by a (0001) top facet and  $\{11\bar{2}0\}$  side facets, while  $\{1\bar{1}01\}$  side facets bound the triangular cross section stripes. We have observed that flat surfaces can be obtained for homoepitaxial films grown with mask stripes oriented along the  $\langle 1\bar{1}00 \rangle$  and that the lateral-to-vertical growth ratio (LTVGR) is as large as  $\sim 2.0$  for this orientation. For stripes oriented along  $\langle 11\bar{2}0 \rangle$ , the growth in the lateral direction is limited by the slow-growing  $\{1\bar{1}01\}$  facets, leading to the narrow triangular cross section typical of growth bounded by slow-growing planes. Using atom-force microscopy, we have measured a RMS roughness as low as  $\sim 0.1$  nm on the top of the flat mesas for stripes parallel to  $\langle 1\bar{1}00 \rangle$ . For comparison, the GaN film grown in the large-area "open" region of the mask at the wagon-wheel hub also has an RMS roughness of  $\sim 0.1$  nm. The facet

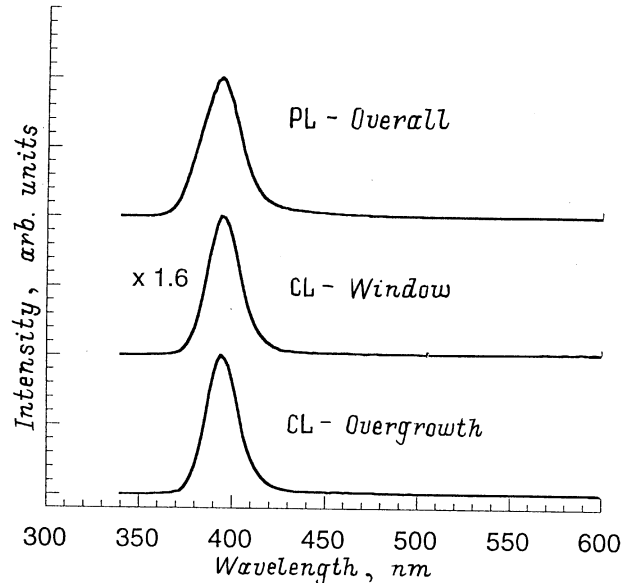


**Figure 6.** Room-temperature cathodoluminescence spectra for InGaIn film grown on GaN SALEO "substrate". The CL from the LEO region is 1.6 times the peak intensity of the SAE region.

sidewalls are found to be more vertical and the mesas are smoother for higher GaN growth temperatures  $\sim 1100^\circ\text{C}$ .

The high-resolution scanning cathodoluminescence (CL) images (300 K) for undoped and Si-doped GaN SALEO mesas indicate that the intensity of the near-band-edge emission is more uniform and about a factor of 2–3 times higher for the GaN:Si LEO region grown over the  $\text{SiO}_2$  mask compared to the GaN homoepitaxial SAE region grown between the mask stripes. The CL linewidths and peak wavelengths are essentially the same for all areas of the wafer. Also, the yellow-band emission is reduced relative to the band-edge emission for the LEO region. This may indicate that a higher density of non-radiative traps exists in the SAE region compared to the LEO material [21]. Initial plan-view and cross-section transmission electron microscope characterization of these materials supports this interpretation and has shown that there are  $\sim 5 \cdot 10^8\ \text{cm}^{-2}$  threading dislocations in the SAE portion of the film; however, no threading dislocations are observed in the LEO portion of the film [22]. The CL emission spectra for the InGaIn film grown on the GaN SALEO film are shown in Fig. 6. The peak intensity is brighter from the region corresponding to growth over the mask while the wavelength and FWHM are somewhat reduced for the SAE compared to the LEO regions. These results show promise for the application of SALEO to improved nitride devices.

### 3. Summary and conclusions

We have shown that MOCVD process can produce high-quality AlGaIn/InGaIn/GaN heterostructure films and we have optimized the properties of the MQW structures. These structures have operated as pulsed lasers at 300 K. In

addition, we have employed the SALEO process to produce GaN films on sapphire substrates with no apparent threading dislocations. The SALEO process can be repeated two or more times to produce a high-quality epitaxial film which is free of threading dislocations from the GaN underlying heteroepitaxial film.

We acknowledge useful technical discussions with Dr. R.F. Karlicek and Dr. C.P. Kuo. We thank D.E. Dupuis for assistance in manuscript preparation.

This work was partially supported by the National Science Foundation under grant DMR-93-12947 and by the NSF Science and Technology Center Program under grant CHE-89-20120, the State of Texas Advanced Technology Program, the Army Research Office under DAAH04-93-G-0317, by ONR under contract NOOO14-95-1-1302, and by DARPA under contract MDA972-95-3-0008. Additional support by Ford Motor Company is also gratefully acknowledged. One of the authors (CJE) thanks the United States Air Force for support under the Palace Knights Program.

## References

- [1] I. Akasaki, H. Amano, Y. Koide, K. Hiramatsu, N. Sawaki. *J. Cryst. Growth*, **98**, 209 (1989).
- [2] I. Akasaki, H. Amano. *J. Electrochem. Soc.*, **141**, 2266 (1994).
- [3] S. Nakamura, M. Senoh, N. Iwasa, S. Nagahama. *Japan. J. Appl. Phys.*, **34**, L797 (1995).
- [4] S. Nakamura, M. Senoh, S. Nagahama, N. Iwasa, T. Yamada, T. Matsushita, H. Kiyoku, Y. Sugimoto. *Japan. J. Appl. Phys.*, **35**, L74 (1996).
- [5] S. Nakamura, M. Senoh, S. Nagahama, N. Iwasa, T. Yamada, T. Matsushita, H. Kiyoku, Y. Sugimoto. *Japan. J. Appl. Phys.*, **35**, L217 (1996).
- [6] S. Nakamura, M. Senoh, S. Nagahama, N. Iwasa, T. Yamada, T. Matsushita, Y. Sugimoto, H. Kiyoku. *Appl. Phys., Lett.*, **70**, 1417 (1997).
- [7] I. Akasaki, H. Amano, S.Sota, H. Sakai, T. Tanaka, M. Koike. *Japan. J. Appl. Phys.*, **34**, L1517 (1995).
- [8] K. Itaya, M. Onomura, J. Nishio, L. Sugiura, S. Saito, M. Suzuki, J. Rennie, S. Nunoue, M. Yamamoto, H. Fujimoto, Y. Kokubun, Y. Ohba, G. Hatakoshi, M. Ishikawa. *Japan. J. Appl. Phys.*, **35**, L1315 (1996).
- [9] G.E. Bulman, K. Doverspike, S.T. Sheppard, T.W. Weeks, M. Leonard, H.S. Kong, H. Dieringer, C. Carter, J. Edmond, J.D. Brown, J.T. Swindell, J.F. Schetzina, Y.-K. Song, M. Kuball, A. Nurmikko. *Device Research Conference and Electronic Materials Conference* (Ft. Collins, Co., 1997).
- [10] Q. Chen, M.A. Khan, C.J. Sun, J.W. Yang. *Appl. Phys. Lett.*, **31**, 1781 (1995).
- [11] J.C. Carrano, P.A. Grudowski, C.J. Eiting, R.D. Dupuis, J.C. Campbell. *Appl. Phys. Lett.*, **70**, 1992 (1997).
- [12] Z. Fan, S.N. Mohammad, O. Aktas, A.E. Botchkarev, A. Salvador, H. Morkoc. *Appl. Phys. Lett.*, **69**, 1229 (1996).
- [13] S. Yoshida, S. Misawa, S. Gonda. *J. Appl. Phys.*, **63**, 6844 (1982).
- [14] B.D. Joyce, J.A. Bradkey. *Nature*, **195**, 458 (1962).
- [15] See A.D. Morrison, T. Daud. US Patent No. 04522661, for a discussion of the application of SALEO to the growth of high-purity semiconductors.
- [16] R.F. Davis. *Gordon Conf. Electronic Materials: Chemistry, Excitations, and Processing* (Henniker, New Hampshire, 1997) (invited paper, unpublished).
- [17] O.H. Nam, M.D. Bremser, T.S. Zheleva, R.F. Davis. *Appl. Phys. Lett.*, **71**, 2638 (1997).
- [18] T.S. Zheleva, O.H. Nam, M.D. Bremser, R.F. Davis. *Appl. Phys. Lett.*, **71**, 2472 (1997).
- [19] S. Nakamura, M. Senoh, S. Nagahama, N. Iwasa, T. Yamada, T. Matsushita, H. Kiyoku, Y. Sugimoto, T. Kozaki, H. Umemoto, M. Sano, K. Chocho. *Appl. Phys. Lett.*, **72**, 211 (1998).
- [20] S. Nakamura. *The 24th International Symposium on Compound Semiconductors* (San Diego CA, 1997) paper plenary 1.
- [21] J. Park, P.A. Grudowski, C.J. Eiting, R.D. Dupuis. *Appl. Phys. Lett.*, **73**, 333 (1998).
- [22] J. Park, P.A. Grudowski, C.J. Eiting, R.D. Dupuis, Z. Liliental-Weber (unpublished).

Редактор Л.В. Шаронова